Static structure factors of binary suspensions of charged polystyrene spheres: experiment against theory and computer simulation

1991 J. Phys.: Condens. Matter 3 4459

(http://iopscience.iop.org/0953-8984/3/24/015)

J. Phys.: Condens. Matter 3 (1991) 4459–4475. Printed in the UK

Static structure factors of binary suspensions of charged polystyrene spheres: experiment against theory and computer simulation

R Krause, B D'Aguanno, J M Méndez-Alcaraz, G Nägele, R Klein and R Weber

Fakultät für Physik, Universität Konstanz, Postfach 5560, 7750 Konstanz, Federal Republic of Germany

Received 25 February 1991

Abstract. The microscopic static structure of dilute binary colloidal suspensions, for compositions covering the full molar fraction range, are investigated using static light scattering experiments. The mixtures of liquid-like ordered suspensions are made from charged polystyrene particles having averaged radii of 42 nm and 65 nm. The data are compared with the results of integral equation theories using the extended re-scaled mean spherical approximation and the hypernetted chain approximation and Rogers–Young closure schemes, and to Monte Carlo computer simulations. The values of charges needed in the Yukawa-type pair potentials are determined from fits to the scattering data of the pure components, and they are kept constant for the mixtures. Of the various theoretical schemes used, the Rogers–Young method is found to be the most satisfactory. In order to fully describe the experimental data, it is necessary to take the intrinsic polydispersity of the two pure components into account.

1. Introduction

Although a lot of work has been done on the microscopic structure of monodisperse colloids [1–6], much less is known in the case of colloidal mixtures or, more generally, in the case of polydisperse systems [7–9]. The reason for this is the increased complexity of their description, both from the experimental and theoretical points of view. But if this complexity can properly be taken into account, the study of mixtures becomes more appealing due to the appearance of new phenomena (i.e. new types of microscopic order, new types of phase behaviour, etc) which are not present in monodisperse suspensions.

Restricting ourselves to the case of binary mixtures of strongly interacting colloidal particles, new questions concerning the dependence of relevant statistical mechanical quantities (like the partial pair distribution functions and the partial static structure factors) on the molar fractions of both components can be addressed. It is our aim to study systematically prototypes of binary mixtures of charged colloidal particles (polystyrene macro-ions of diameters $\sigma_1 = 84$ nm, $\sigma_2 = 130$ nm and effective charges of the order of some hundreds of electrons) in the full range of molar fractions, ranging from one pure component to the other. The total volume fraction of the mixture is chosen such that the systems remain well inside the liquid phase ($\Phi_T \approx 5 \times 10^{-4}$), and it is kept nearly constant.

0953-8984/91/244459+17$03.50

Like the monodisperse colloidal suspensions, the binary mixtures can be experimentally studied using static light scattering (SLS) techniques. However, the quantity that is measured in binary mixtures, namely the measured static structural factor $S^M(q)$, reflects both the correlations between the two species and the intraparticle scattering properties. These last contributions, which do not appear in $S^M(q)$ in the case of monodisperse suspensions, destroy the usual statistical mechanical interpretation of the main features of $S^M(q)$. For example, $S^M(q = 0)$ can no longer be interpreted as the isothermal compressibility of the system, the peak position of $S^M(q)$ is no longer simply related to the mean interparticle distance, etc.

The theoretical interpretation of the SLS data can be performed using integral equation theories like the extended rescaled mean spherical approximation (RMSA) [7, 8], the hypernetted chain approximation (HNC) and the Rogers–Young closure [9]. In addition, the data can also be analysed performing Monte Carlo (MC) computer simulations. The interaction potential, which is needed in these schemes, is modelled according to the repulsive part of the well-known DLVO potential: a Yukawa-type pair interaction. In contrast to the monodisperse suspensions, the analysis of SLS data of binary mixtures requires a further model concerning the single-particle scattering mechanism. We consider the particles as spheres of homogeneous scattering material with a certain refractive index, n_p, independent of the particle size.

The parameters entering the theoretical schemes are the total density, the molar fraction of one component, the particle diameters, the effective particle charges and the temperature, which determine the DLVO potential. While the former parameters are accessible experimentally, the effective charges are difficult to measure; to determine them, we apply the fitting procedure to the peak value of the measured structural factor of the pure components.

In this work, trends of several features of $S^M(q)$ are identified and analysed using the concept of charge and size bidispersities, as the molar fraction range is fully exploited. In particular, this concept explains the systematic variation of the peak height and position of $S^M(q)$ as a function of the molar fraction. However, the charge and size bidispersities alone are not sufficient to fully interpret the SLS data. These data are definitely also affected by the intrinsic and unavoidable charge and size polydispersity of each of the components. To introduce the intrinsic polydispersity in the theoretical approaches, we construct a model in which the two pure components are represented by a discretized version of the continuous Schulz distribution. In this way, a quantitative agreement with the measured structural factors is found.

The paper is organized as follows. The static light scattering relations, the experimental equipment, the sample preparations and the measurements are described in section 2. In section 3 we describe the MC simulations, the RMSA, the HNC and the RY integral equations for the determination of the static structure functions. Section 4 is devoted to the presentation of the results and to the comparison of the experimental data with the theoretical findings. Finally, the conclusions are summarized in section 5.

2. Scattering relations and experimental details

It is worthwhile to begin by giving some introduction to the method of performing static light scattering experiments, to the technical details of the light scattering setup, to the sample preparation and to the sample characterization.

In a static light scattering experiment, the measured averaged scattered intensity from a sample having p different kinds of scattering spheres is given by

$$I(q) = \left\langle \left| \sum_{\alpha=1}^{p} \sum_{i=1}^{N_\alpha} b_\alpha(q) \exp(\mathrm{i}\boldsymbol{q}\boldsymbol{r}_i^\alpha) \right|^2 \right\rangle \tag{1}$$

where N_α is the number of particles of type α, $b_\alpha(q)$ is the corresponding scattering amplitude, q is the magnitude of the scattering wavevector $\boldsymbol{q}$, and $\boldsymbol{r}_i^\alpha$ is the position of particle i of type α. Considering a unit volume of the sample, this relation can always be written as

$$I(q) = n\overline{P(q)}S^{\mathrm{M}}(q) \tag{2}$$

where n is the total number density of the sample, $\overline{P(q)}$ is the averaged form factor and $S^{\mathrm{M}}(q)$ is the measured structural factor that contains information about the interparticle correlations of the sample. For spherical particles of homogeneous scattering material, the averaged form factor, apart from a constant, is

$$\overline{P(q)} = \sum_{\alpha=1}^{p} x_\alpha b_\alpha^2(q) \tag{3}$$

where $x_\alpha = n_\alpha/n$ is the molar fraction of species α and

$$b_\alpha(q) = V_{\mathrm{p}}^\alpha (n_{\mathrm{p}}^\alpha - n_{\mathrm{s}}) \frac{3j_1(q\sigma_\alpha/2)}{q\sigma_\alpha/2} \tag{4}$$

where V_{p}^α is the volume of an α-particle, n_{p}^α and n_{s} are the refractive indices of the α-particles and of the solvent, respectively, j_1 is the first-order spherical Bessel function and σ_α is the α-particle diameter. In what follows, we assume that n_{p}^α is independent of the size of the spheres.

The measured structural factor is defined by the relation

$$S^{\mathrm{M}}(q) = \frac{1}{\overline{P(q)}} \sum_{\alpha=1}^{p} \sum_{\beta=1}^{p} b_\alpha(q) b_\beta(q) S_{\alpha\beta}(q) \tag{5}$$

where

$$S_{\alpha\beta}(q) = \frac{1}{N} \sum_{i=1}^{N_\alpha} \sum_{j=1}^{N_\beta} \left\langle \exp(\mathrm{i}\boldsymbol{q}(\boldsymbol{r}_i^\alpha - \boldsymbol{r}_j^\beta)) \right\rangle = x_\alpha \delta_{\alpha\beta} + n x_\alpha x_\beta \tilde{h}_{\alpha\beta}(q) \tag{6}$$

are the partial structural factors. Here, $\tilde{h}_{\alpha\beta}(q)$ is the Fourier transform of the total correlation function $h_{\alpha\beta}(r)$ and N is the total number of particles.

For a non-interacting system of density n_0, the total correlation functions $\tilde{h}_{\alpha\beta}(q)$ go to zero and the measured structural factor approaches unity: this is obvious from equations (5) and (6). The corresponding measured intensity becomes

$$I_0(q) = n_0 \overline{P(q)}. \tag{7}$$

For a two-component system, the measured structural factor, obtained directly from a SLS experiment, is given by

$$S^{M}(q) = \frac{I(q)}{I_0(q)}\frac{n_0}{n}$$
$$= \frac{1}{\overline{P(q)}}[b_1^2(q)S_{11}(q) + b_2^2(q)S_{22}(q) + 2b_1(q)b_2(q)S_{12}(q)]. \quad (8)$$

Although the second line of this equation is relevant to the theoretical determination of $S^{M}(q)$, the first line shows how $S^{M}(q)$ is determined in the SLS experiment.

To characterize the particles, we performed dynamic light scattering (DLS) experiments on very dilute samples of each of the two componets. The fact that the dynamic correlation functions exhibit a finite second cumulant K_2 shows that the so-called pure components are, to some extent, polydisperse. From the cumulant analysis [10, 11] we determined the standard deviations $s_{1,2}$ of the particle sizes using the relation $s = K_2/K_1^2$, where K_1 is the first cumulant. It is with this qualification that we use the word 'monodisperse' when speaking about the samples having $x_1 = 0$ and $x_1 = 1$. For them, we obtained the values $s_{1,2} = 0.1 \pm 0.02$. The dynamic light scattering experiments have been made in the homodyne mode.

We used a light scattering apparatus (ALV, FRG) consisting of: (*a*) a computer-controlled goniometer table with focussing and detector-optics; (*b*) a stabilized-power 3 W argon laser (Spectra Physics); (*c*) a 4-bit real-time correlator (1023 channels); (*d*) a digital rate meter and (*e*) a temperature control which stabilized the temperature of the sample cell at $T = (21 \pm 1)\,^{\circ}\mathrm{C}$. Intensity data were corrected for the dark current rate of the photomultiplier and by the angle dependence of the scattering volume. The magnitude of the scattering vector

$$q = \frac{4\pi n_s}{\lambda_0}\sin(\Theta/2) \quad (9)$$

ranges from $3\times10^{-3}\,\mathrm{nm}^{-1}$ to $33\times10^{-3}\,\mathrm{nm}^{-1}$ at the vacuum wavelength of the incident light $\lambda_0 = 488\,\mathrm{nm}$ in aqueous solutions with a solvent refractive index $n_s = 1.33$. The beam first passed an index-matched fluid (silicon oil) and then entered the scattering cell, where it was focussed into the scattering volume. We used quartz tubes of 10 mm outer diameter as scattering cells.

All measurements were normalized to a reference sample (toluene) in the whole q region to correct laser power fluctuations and to get a standard of the incident light intensity.

To have a higher resolution of the scattered intensity data within the region of the first maximum, we measured the scattering angles, up to the second maximum, by steps of 1° and, in special cases, by steps of 0.5°. The region where we expected to be on the plateau of the measured structural factor ($S^{M}(q) \approx 1$) was scanned with a resolution of 3°.

The salt-free monodisperse and bidisperse samples are listed in table 1. The samples are diluted from highly concentrated polystyrene solutions (Dow Chemicals) using de-ionized water. The 10 bidisperse samples are prepared starting from two well-characterized purely monodisperse batches of polystyrene spheres with average diameters $\sigma_1 = 84$ nm and $\sigma_2 = 130$ nm. The partial volume fractions $\Phi_\alpha^{exp} = \pi n_\alpha \sigma_\alpha^3/6$, $\alpha = 1, 2$, are also listed in table 1.

Table 1. Volume fractions of all 12 samples under study. The method to obtain $\Phi_{1,2}^{fit}$ *and* x_1^{fit} *is explained in section 4.*

Sample	Φ_1^{exp}	Φ_2^{exp}	Φ_1^{fit}	Φ_2^{fit}	x_1^{fit}
1	—	5.0×10^{-4}	—	4.5×10^{-4}	0
2	5×10^{-5}	4.5×10^{-4}	5.3×10^{-5}	4.05×10^{-4}	0.326
3	1×10^{-4}	4×10^{-4}	9.5×10^{-5}	3.6×10^{-4}	0.494
4	1.5×10^{-4}	3.5×10^{-4}	1.5×10^{-4}	3.15×10^{-4}	0.638
5	2×10^{-4}	3×10^{-4}	2×10^{-4}	2.7×10^{-4}	0.733
6	2.5×10^{-4}	2.5×10^{-4}	2.5×10^{-4}	2.25×10^{-4}	0.804
7	2.85×10^{-4}	2.15×10^{-4}	3.1×10^{-4}	1.93×10^{-4}	0.856
8	3×10^{-4}	2×10^{-4}	3.5×10^{-4}	1.8×10^{-4}	0.878
9	3.5×10^{-4}	1.5×10^{-4}	3.85×10^{-4}	1.35×10^{-4}	0.913
10	4×10^{-4}	1×10^{-4}	4.9×10^{-4}	9×10^{-5}	0.952
11	4.5×10^{-4}	5×10^{-5}	5.55×10^{-4}	4.5×10^{-5}	0.978
12	5×10^{-4}	—	6.2×10^{-4}	—	1

To minimize the ionic strength of the suspension, a cleaned mixed-bed ion exchange resin was added to the samples, removing all small ions other than H^+ and OH^-. No investigations with added salt were made, since we were only interested in systems with strong Coulomb interactions.

For the determination of the effective charges on the macro-ions, we prefer to obtain these values fitting the peak height of the measured structural factor by MC computer simulation and by integral equation theories. The direct experimental determinations of such quantities, by conductivity measurements and by pH measurements, produce data that are not yet fully reliable. A summary of the parameters characterizing the systems used in this study is given in tables 1 and 2.

Table 2. Parameters characterizing the macro-ions of the pure components.

Species	Z^{MC}	Z^{RMSA}	Z^{HNC}	Z^{RY}	σ [nm]
1	330	450	438	373	84
2	280	325	323	288	130

The concentrations were also checked by MC computer simulations and by integral equation theory, fitting once more the position of the first maximum of $S^M(q)$ [12].

3. Theory

3.1. Monte Carlo computer simulation

To perform Monte Carlo computer simulations of dilute binary suspensions of charged polystyrene spheres within the framework of the two-component macro-ion fluid (TCM), we used the following pair potential

$$\frac{U_{\alpha\beta}(r)}{k_B T} = \begin{cases} +\infty & \text{if } r < \sigma_{\alpha\beta} = \frac{\sigma_\alpha + \sigma_\beta}{2} \\ A_\alpha^{DLVO} A_\beta^{DLVO} e^{-\kappa r}/r & \text{if } r > \sigma_{\alpha\beta} \end{cases} \tag{10}$$

with

$$A_\alpha^{\mathrm{DLVO}} = L_B^{1/2} \frac{Z_\alpha \exp(\kappa\sigma_\alpha/2)}{1+\kappa\sigma_\alpha/2} \tag{11}$$

which is the repulsive part of the well-known DLVO potential. Here Z_α is the valence of α macro-ion, $L_B = \exp(2/\epsilon k_B T)$ is the Bjerrum length and κ the inverse Debye screening length. In salt-free systems, κ is determined only by the monovalent counterions as

$$\kappa^2 = 4\pi L_B n \sum_{\alpha=1}^{2} x_\alpha Z_\alpha. \tag{12}$$

The MC simulations were carried out using the standard Metropolis algorithm [13, 14] with $N = N_1 + N_2 = 864$ particles. The other parameters included in the interaction potential are chosen case by case, in order to make comparisons with the SLS data.

From the simulations we computed the measured static structural factor $S^M(q)$, defined in (8), using the procedure suggested by Frenkel *et al* [15]. More precisely, $S^M(q)$ is computed rewriting equation (8), using (1), as

$$S^M(q) = \left(\sum_{i=1}^{N_1+N_2} b_i^2(q)\right)^{-1} \left\langle \left[\sum_{i=1}^{N_1+N_2} b_i(q)\cos \boldsymbol{q}\boldsymbol{r}_i\right]^2 + \left[\sum_{i=1}^{N_1+N_2} b_i(q)\sin \boldsymbol{q}\boldsymbol{r}_i\right]^2 \right\rangle \tag{13}$$

in which

$$b_i(q) = \begin{cases} b_1(q) & \text{for } i = 1,\ldots,N_1 \\ b_2(q) & \text{for } i = N_1+1,\ldots,N \end{cases}$$

is calculated according to (4). To decrease statistical fluctuations in $S^M(q)$, the vector q is taken along three independent directions, namely the permutations of [100].

This procedure saves substantial computing time as compared with first evaluating the partial structural factors $S_{\alpha\beta}(q)$ and then calculating $S^M(q)$ using (5). Secondly, this procedure is not affected by the truncation errors typical of finding the direct Fourier transform of $g(r)$.

3.2. Extended rescaled mean spherical approximation

In this section, the rescaled mean spherical approximation (RMSA) for colloidal mixtures interacting via a Yukawa-type pair potential is presented, and its application to suspensions of highly charged polystyrene spheres is illustrated. Since the details of the extended RMSA have already been reported [7], we only summarize its salient features needed for our further discussion.

The three partial radial distribution functions $g_{\alpha\beta}(r)$ and partial static structural factors can be determined from the Ornstein–Zernike (OZ) equations

$$g_{\alpha\beta}(r) - 1 = c_{\alpha\beta}(r) + \sum_{\gamma=1}^{2} n_\gamma \int d^3r'\, c_{\alpha\gamma}(|\,\boldsymbol{r}-\boldsymbol{r}'\,|)[g_{\gamma\beta}(r') - 1] \tag{14}$$

in connection with specific closure relations for the direct correlation functions $c_{\alpha\beta}(r)$. This has to be supplemented with the rigorous boundary conditions

$$g_{\alpha\beta}(r) = 0 \qquad r < \sigma_{\alpha\beta} \tag{15}$$

which state that two hard spheres cannot interpenetrate. The MSA closure relation

$$c_{\alpha\beta}(r) = -\frac{U_{\alpha\beta}(r)}{k_B T} \qquad r > \sigma_{\alpha\beta} \tag{16}$$

has found special attention, since it can be solved analytically for a Yukawa-type pair potential as given in (10).

The MSA can lead to non-physical negative values of the $g_{\alpha\beta}(r)$ close to the contact distance of two spheres in diluted and strongly interacting systems. In fact, to zeroth order in concentration of both species

$$g_{\alpha\beta}^{\mathrm{MSA}}(r) = 1 - A_\alpha^{\mathrm{DLVO}} A_\beta^{\mathrm{DLVO}} \, \mathrm{e}^{-\kappa r}/r \qquad r > \sigma_{\alpha\beta} \tag{17}$$

which becomes negative for large coupling parameters.

To overcome this feature, Hansen and Hayter [16] provide physical arguments for one-component repulsive Yukawa systems leading to the well-known rescaled mean spherical approximation. This RMSA procedure has been widely used for the interpretation of light scattering data of monodisperse samples [12, 17, 18, 19].

In a recent paper, Ruiz-Estrada *et al* [7] extended Hansen and Hayter's MSA rescaling arguments to mixtures of hard spheres interacting through long range repulsive Yukawa potentials with factorized coupling parameters.

In this extension, the analytic MSA solution of the system of interest is combined, with the rescaling argument, with systems where the MSA radial distribution functions are negative close to the contact distance. According to this argument the physical diameters σ_α are enlarged to rescaled values $\sigma'_\alpha > \sigma_\alpha$ determined from $g_{\alpha\alpha}(r = \sigma'_\alpha +) = 0$, i.e. determined in such a way that $g_{\alpha\alpha}(r)$ approaches zero for $r \to \sigma_\alpha +$ without showing a discontinuity. The values of the pair potential are kept constant, i.e. the coupling amplitudes A_α^{DLVO} and the screening parameter κ are kept fixed while increasing the diameter from σ_α to σ'_α.

We remark that, due to the additivity of the diameters in the MSA solution, there is no guarantee that $g_{12}(r = \sigma'_{12} +) = 0$ holds exactly. It is observed, however, that $g_{12}(\sigma'_{12} +) \approx 0$ for all practical purposes, as long as the asymmetry in the sizes and charges of the two macro-ion species is not too extreme [7, 8].

The pair correlation functions are not calculated by directly solving equations (14)–(16). Instead of this, a method of MSA solution for the Yukawa system is established, based on the transformation of the original problem into the mathematically equivalent (but much easier) problem of determining the MSA partial structural factors of a corresponding primitive model system with point-like counter-ions.

A comparison of the extended RMSA radial distribution functions with computer simulation data of Kremer *et al* [20, 21] is quite satisfactory as far as the distance of closest approach and the prediction of the position of the maxima and minima are concerned [8]. However, the RMSA somewhat underestimates some quantities, especially the height of the first maximum of $g_{\alpha\beta}(r)$. This is a feature that the extended RMSA for mixtures shares with the well-known RMSA in the monodisperse case. The underestimation of the peak height is, however, only appreciable in strongly coupled systems.

3.3. Hypernetted chain and Rogers–Young approximation

The problem of adjusting the coupling parameters in the RMSA in a somewhat arbitrary way can be largely overcome if the OZ equations are solved using other closure relations. Of particular relevance are the hypernetted chain (HNC) [13] and Rogers–Young (RY) [22] closures. As compared to the rescaled mean spherical approximation, which is a linear closure, the HNC and RY are treating the direct correlations in a nonlinear, and improved way, as functions of the interaction potential. However, this more appropriate description of the correlations requires a numerical implementation of the HNC and RY schemes, in contrast to the RMSA.

For a multicomponent system, the HNC closure is

$$h_{\alpha\beta}(r) = -1 + \exp[-\beta U_{\alpha\beta}(r) + h_{\alpha\beta}(r) - c_{\alpha\beta}(r)] \qquad \alpha, \beta = 1, \ldots\ldots, p \tag{18}$$

where $\beta = (k_B T)^{-1}$ and $c_{\alpha\beta}(r)$ is the direct correlation function.

The RY closure is given by

$$h_{\alpha\beta}(r) = -1 + \exp[-\beta U_{\alpha\beta}(r)] \left(1 + \frac{\exp(f(r)[h_{\alpha\beta}(r) - c_{\alpha\beta}(r)]) - 1}{f(r)}\right). \tag{19}$$

The function

$$f(r) = 1 - \exp(-\gamma r) \tag{20}$$

depends on the mixing parameter γ; this parameter is changed in the numerical solution of the RY and OZ equations, in order to get at least partial thermodynamic consistency [2]. The RY approximation, which gives better results than HNC and RMSA when compared with MC simulation data [9, 23], is, however, more time-consuming than the other schemes. The details of the numerical solutions of the RY and HNC schemes for a multicomponent Yukawa system are given in recent publications [9, 23].

We applied these integral equation methods to a two-component Yukawa system in which each component is assumed to be monodisperse, and to a two-component Yukawa system in which each component is assumed to be polydisperse either in size and in charge.

In this last case, the distributions of particle sizes and charges of each component are represented by a histogrammatic reduction of the continuous Schulz distribution [9]. In fact, it is well-known that the measured size distribution can be well fitted using such a distribution [24, 25]. It is given by

$$f(\sigma) = \left(\frac{t+1}{\langle\sigma\rangle}\right)^{t+1} \frac{\sigma^t}{\Gamma(t+1)} \exp\left[-\frac{t+1}{\langle\sigma\rangle}\sigma\right] \qquad (t > 0) \tag{21}$$

where t is a measure of the width of the distribution, $\Gamma(t)$ is the gamma function and $\langle\sigma\rangle$ is the mean value or first moment of the distribution.

Figure 6 shows the model used to treat the intrinsic polydispersity of each component. The positions and the weights of each three-component histogram are determined equating the first six moments of the histogrammatic and continuous distributions. We expect that this model should be effective in describing structural and thermodynamical properties since Vrij [26] showed that a polydisperse hard sphere system, treated within the Percus–Yevick approximation, is fully characterized by the first six moments of the size distribution.

4. Results

In this section we compare our SLS data obtained for the 12 samples, whose parameters are summarized in tables 1 and 2, with the corresponding computer simulation data and with the integral equation results.

Binary samples of particles having diameters $\sigma_1 = 84$ nm and $\sigma_2 = 130$ nm have been prepared for different values of the mole fraction $x_1 = n_1/(n_1 + n_2)$. The total volume fractions $\Phi_T = \Phi_1 + \Phi_2$ of the different samples have been chosen such that the measured structural factor, given in (8), describes the normalized scattering function of a binary system located well within the homogeneous liquid phase. Table 1 lists the volume fractions of both components and the molar fractions of component 1 for all 12 samples studied. The fitted values of the volume fractions, Φ_α^{fit}, have been determined by fitting $S^{theory}(q)$ to the position of the main peak of $S^{SLS}(q)$. All the four different theoretical approaches (RMSA, HNC, RY, MC) gave for each sample the same values of Φ_α^{fit}.

To determine the effective charges on the macro-ions of species 1 and 2, we fitted the peak height of $S^{theory}(q)$ to the corresponding experimental value of the two pure samples (samples 1 and 12). The results of the fits are summarized in table 2. In this case the three theoretical approaches and the MC simulations give different results for the effective charges. This is not surprising since, in determining the correlation functions, all the previous schemes treat the interaction between the particles in different ways. For example, the RMSA somewhat underestimates the structure of strongly coupled dispersions, as already mentioned above, leading to values of $Z_{1,2}^{RMSA}$ larger than the others. The values of the charges so determined are then used to evaluate the measured static structural factor, $S^M(q)$, in all the other intermediate samples (samples 2 to 11). We also note that the smaller particles have the larger effective charge, but this fact depends only on the macro-ion preparation. The particles of species 1 have sulfate surface groups whereas those of species 2 have carboxylated surface groups; those of the first kind are more easily ionized.

The comparison between SLS data and RMSA fit for the 84 nm macro-ion system (sample 12) is quite satisfactory, i.e. $S^{RMSA}(q)$ provides a rather accurate fit of $S^{SLS}(q)$, although the second and third maxima of $S^{RMSA}(q)$ are slightly shifted to the right, as shown in figure 1. These features of the RMSA have been observed quite generally [12, 27].

The comparison between the theoretical fit and the SLS data for the 130 nm macro-ion system (sample 1) is less satisfactory: the second and third maxima of $S^{theory}(q)$ are largely out of phase. There is a main reason for this less satisfactory agreement and it is of experimental origin. Since the structural features of $S^{SLS}(q)$ of this sample are at considerably lower values of q than those of sample 12, they are affected by larger experimental errors, which arise mainly from reflections of the incident beam from the sample cell.

Keeping fixed the charges $Z_{1,2}^{RMSA}$ determined in the pure samples, the measured structural factors $S^{RMSA}(q)$ are compared with the SLS data at intermediate molar fractions (samples 2 to 11). As can be seen in figure 1, overall agreement is found, although the second maximum is always somewhat out of phase. Further disagreement is also observed at small wavevectors q.

Summarizing, it can be stated that the extended RMSA provides a fast and convenient device to describe (at least qualitatively) the structure of mixtures of highly charged polystyrene spheres.

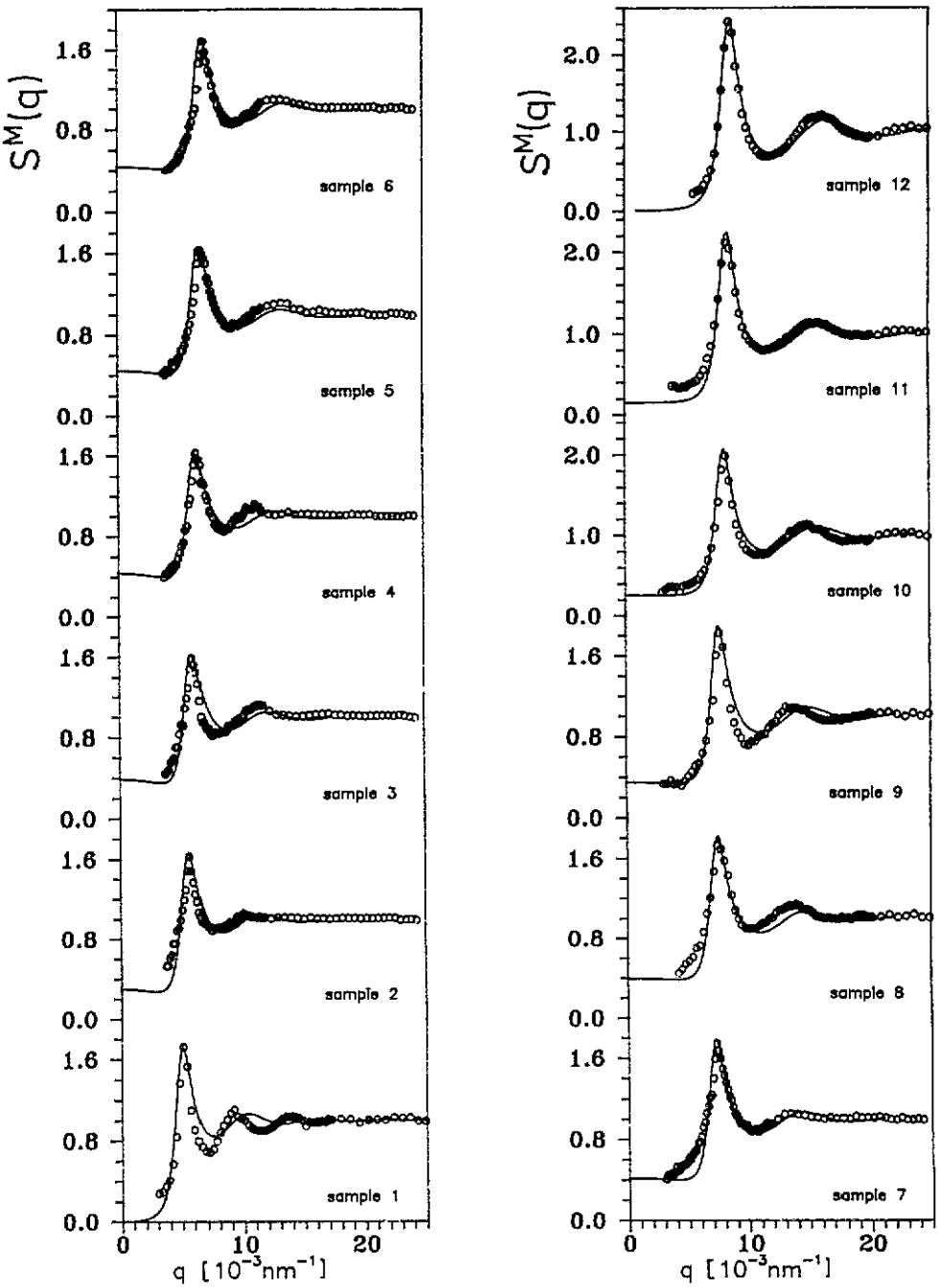

Figure 1. Comparisons between the experimentally measured structural factors (OOO) and those determined with RMSA (——). The system parameters used are given in tables 1 and 2.

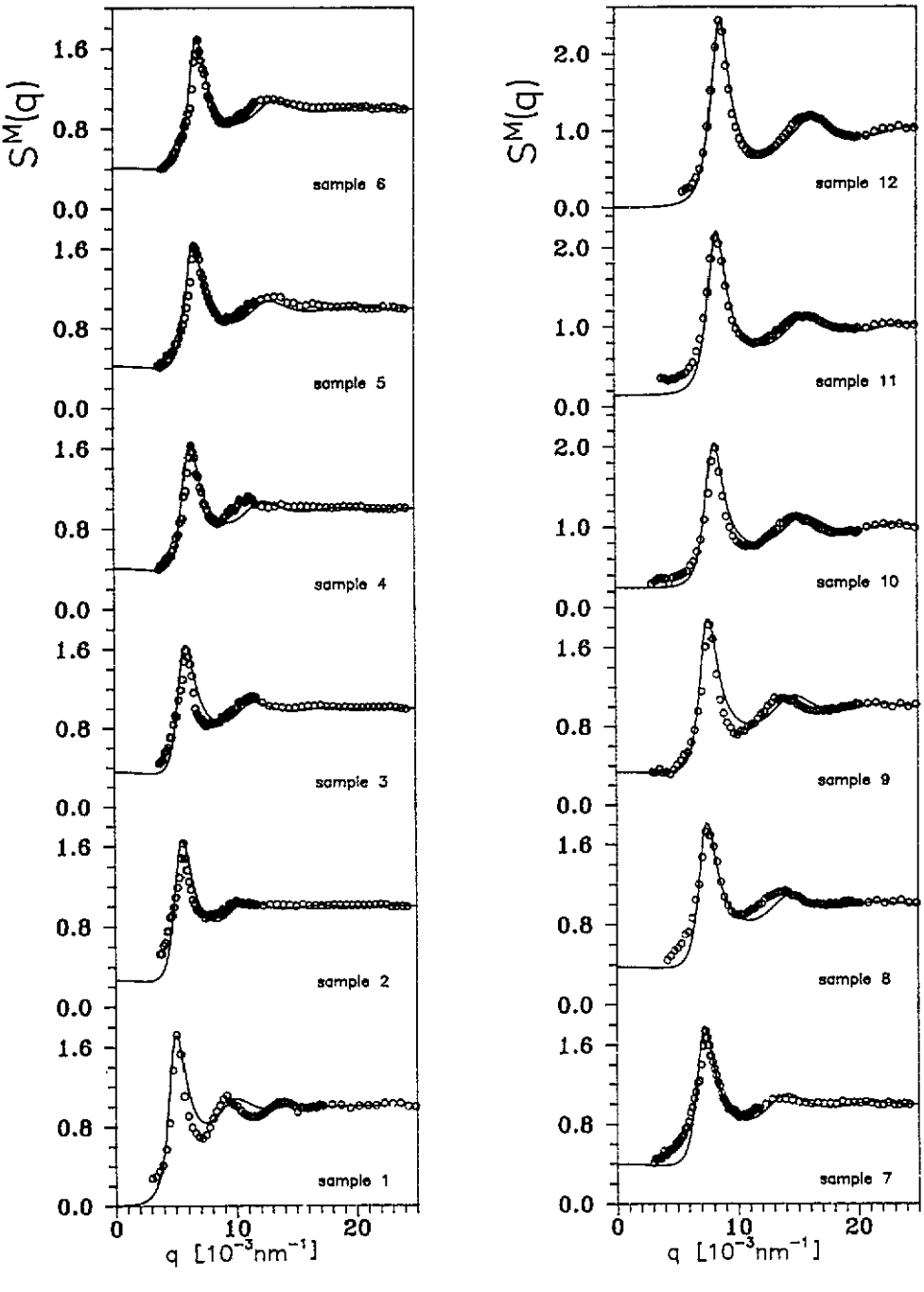

Figure 2. Comparisons between the experimentally measured structural factors (OOO) and those determined with RY (——). The system parameters used are given in tables 1 and 2.

Figure 2 shows comparisons between RY fits and SLS data for the same samples. The fitting procedure is entirely equal to the one sketched for the case of the RMSA. An overall qualitative agreement is found. However, the phase shift after the first maximum of $S^{M}(q)$ and the poor agreement at small q values are still present. In figure 3 we compare MC simulation results with SLS data of sample 3 and 9. For this case, we used the same fitting procedure as before. The overall behaviour of $S^{MC}(q)$ is like that shown by $S^{RY}(q)$.

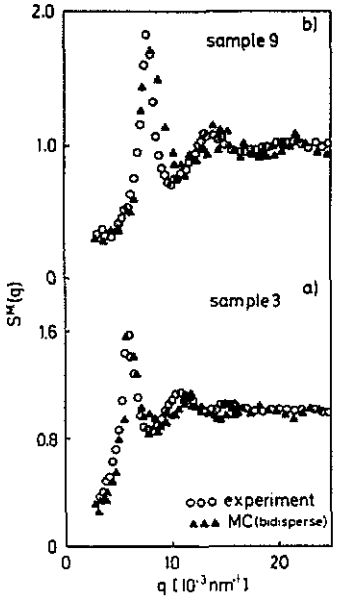

Figure 3. Comparisons between the experimentally measured structural factors (OOO) and those determined with MC computer simulations (▲▲▲). The system parameters used are given in tables 1 and 2. (*a*) sample 3; (*b*) sample 9.

The result of the comparison between $S^{theory}(q)$ and $S^{SLS}(q)$ indicates that a better 'physical description' of the systems is required to recover the experimental data. In what follows, we will show that the introduction of the intrinsic polydispersity of each component is essential in getting a quantitative agreement with the experimental data. Going back to table 2, we see that the effective charges used in the RY fits are more close to those obtained from MC simulation.

After these general observations, we will now comment on some characteristic and important trends that can be extracted from the complete data set. With regard to the behaviour of the peak height of the structural factors as functions of the molar fraction, we show in figure 4 the values of the peak height of $S^{M}(q)$, denoted by S^{M}_{max}, as obtained from the experiments and from the integral equation theories.

We stress once more that the results from the integral equation theories have been obtained fixing once for all the values of the macro-ion charges using a fit for two pure components. No further adjustments have been made as far as the molar fraction is concerned: a good agreement is found. We see also that the experimental data are systematically slightly below the theoretical results. This is due to a finite resolution of the data aquisition (see section 2) so that the experimental values of

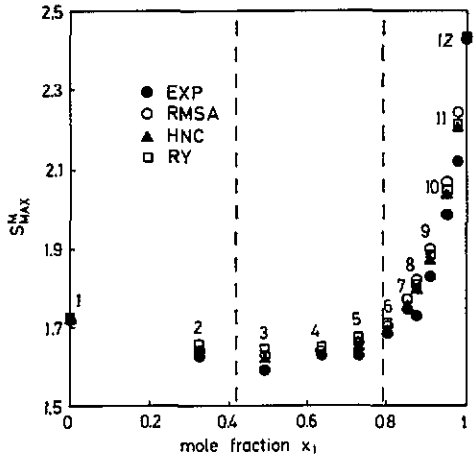

Figure 4. Values of S^M_{max} as measured from SLS experiments and as obtained from RMSA, HNC and RY as functions of the molar fraction x_1.

S^{SLS}_{max} have to be interpreted as a lower limit. The fact that there is this type of systematic behaviour as compared to having S^{SLS}_{max} smaller than the theoretical result for some values of x_1 and larger for other values (see Härtl and coworkers [27]), is very satifactory; it shows that the sample characterization on the one hand and the theoretical schemes on the other hand lead to a consistent description.

The data of S^M_{max} show a minimum around $x_1 \approx 0.5$. This behaviour can be understood in terms of the size and charge bidispersities of all the systems. As shown in previous work by Frenkel *et al* [9] on polydisperse hard sphere systems and by D'Aguanno and Klein [9] on polydisperse Yukawa systems, a maximum in the polydispersity corresponds to a minimum of S^M_{max}. At the same time, it was shown that the amount of polydispersity is closely related to the presence or absence of the structure of $S^M(q)$ beyond the first maximum. This is also observed in figure 1; samples 3 to 6 exhibit less developed structure than the others.

Figure 5 shows the behaviour of the size bidispersities, that is, the diameter bidispersity $s_\sigma = (\langle\sigma^2\rangle - \langle\sigma\rangle^2)/\langle\sigma\rangle^2$ and of the volume bidispersity $s_b = (\langle\sigma^6\rangle - \langle\sigma^3\rangle^2)/\langle\sigma^3\rangle^2$ as functions of x_1, as well as the behaviour of the charge bidispersity $s_Z = (\langle Z^2\rangle - \langle Z\rangle^2)/\langle Z\rangle^2$. Despite the fact that we cannot quantify the way in which each one of these contributions enters into $S^M(q)$ (see equations (4)–(8)), we can use the positions of the maxima of s_σ, s_Z and s_b to estimate a region in x_1 in which S^M_{max} is expected to have its minimum. From figure 5 we see that arbitrary combinations of s_σ, s_Z and s_b reach the maximum in the region $0.4 \leqslant x_1 \leqslant 0.8$. It is this region that contains the observed minimum of S^M_{max} plotted as a function of x_1. The samples that lie in this region also show less pronounced structural features for q values beyond the first maximum of $S^M(q)$ (see figures 1 and 2).

To fully recover the experimental $S^M(q)$, we studied several samples taking into account the intrinsic polydispersity of each component. The model is shown in figure 6, for the specific case of sample 3. Each one of the polydisperse species is replaced by a 3- component histogram with a standard deviation $s_{1,2} = 0.1$ (see section 2). We assumed that the particle sizes obey the Schulz distribution; to construct the histogram we used the procedure given in the previous section.

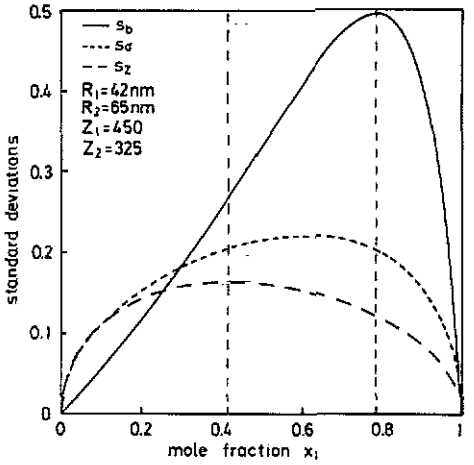

Figure 5. Size bidispersity (----), charge bidispersity (– – –) and volume bidispersity (——) as functions of the molar fraction x_1.

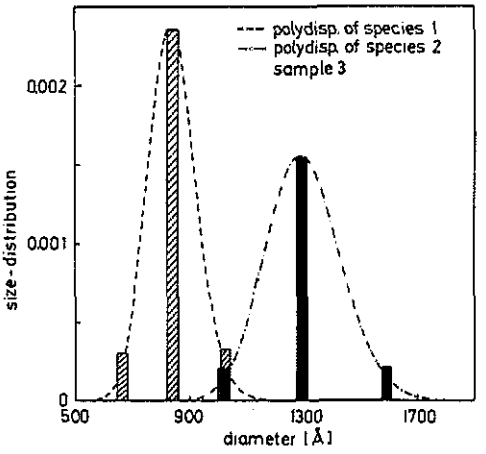

Figure 6. Particle size distributions for sample 3 with the standard deviations $s_1 = s_2 = 0.1$. The 3 vertical stripes in each distribution are the histogrammatic representation of the Schulz distributions (---- and — · —).

Figures 7 (*a–b*) show the results of $S^M(q)$ for both pure samples (samples 1 and 12). The full curves refer to the HNC fits that use the intrinsic polydisperse model, whereas the broken curves refer to the monocomponent model. As expected, the intrinsic polydisperse model describes correctly both the phase behaviour of $S^M(q)$ beyond the first maximum, and the unusually high values at small q.

Figures 8 (*a–c*) show the results of $S^M(q)$ for three intermediate samples (samples 3, 9 and 10) where the polydispersity as determined for the pure samples has been included. In the polydispersity model we assumed that the surface charge of each species is constant. Once again, the intrinsic polydispersity model (full curves) reproduces, with a high accuracy, the measured structural factors. This is particularly true for the improved agreement between the experimental data and the theoretical

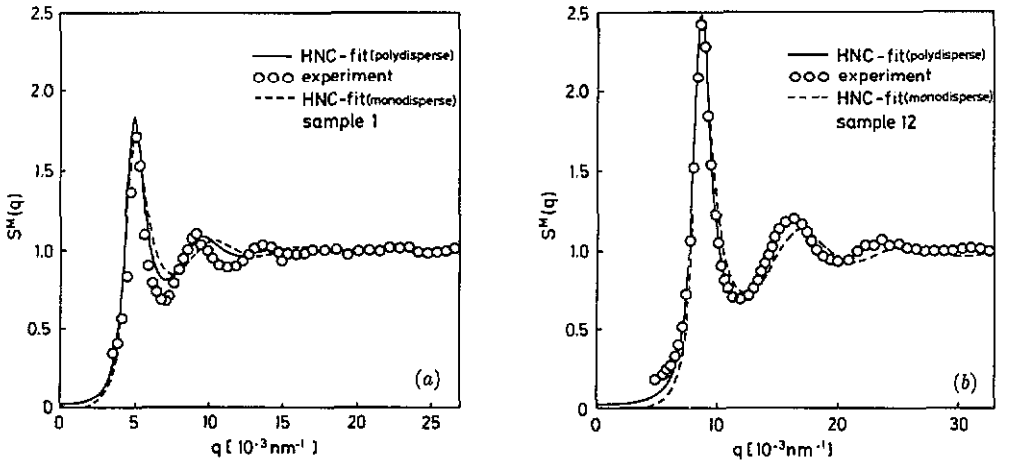

Figure 7. Experimentally measured static structural factor $S^{SLS}(q)$ of the pure sample 1 (o o o), compared with HNC results from the intrinsic polydispersity model with s_1 = 0.1 (——) and the HNC results from the monocompcnent model (----). The system parameters are given in table 3. (*a*) sample 1; (*b*) pure sample 12.

results for q values beyond the first maximum. The behaviour at small q is, in contrast, mainly determined by the bidispersity; here the inclusion of the polydispersity results in only small corrections.

The parameters of these fits are listed in table 3. To recover the experimental $S^M(q)$, we have to increase the values of the volume fractions as well as the values of the charges, since the polydispersity reduces the value of the peak height and shifts the peak position to lower q. This is consistently shown by the fitting parameters of table 3 compared with the corresponding parameters listed in tables 1 and 2.

Table 3. Systems parameters of the two pure samples (1 and 12) and of three bidisperse samples (3, 9 and 10) using intrinsic polydispersity, $s_1 = s_2 = 0.1$, within the HNC closure.

Sample	Φ_1^{HNC}	Φ_2^{HNC}	Z_1^{HNC}	Z_2^{HNC}	x_1
1	—	4.7×10^{-4}	—	400	0
3	9.9×10^{-5}	3.76×10^{-4}	540	400	0.495
9	4.03×10^{-4}	1.41×10^{-4}	540	400	0.914
10	5.13×10^{-4}	9.4×10^{-5}	540	400	0.953
12	6.4×10^{-4}	—	540	—	1

5. Conclusions

This work compares experimentally obtained static structural factors $S^{SLS}(q)$ of dilute binary colloidal suspensions with corresponding MC computer simulations and results from integral equation theories. The static light scattering experiments have been performed on samples of polystyrene spheres of average diameters σ_1 = 84 nm and σ_2 = 130 nm and of volume fractions of the order of $\Phi_T \approx 5 \times 10^{-4}$. All samples were treated by ion exchange resin and were therefore of low salinity.

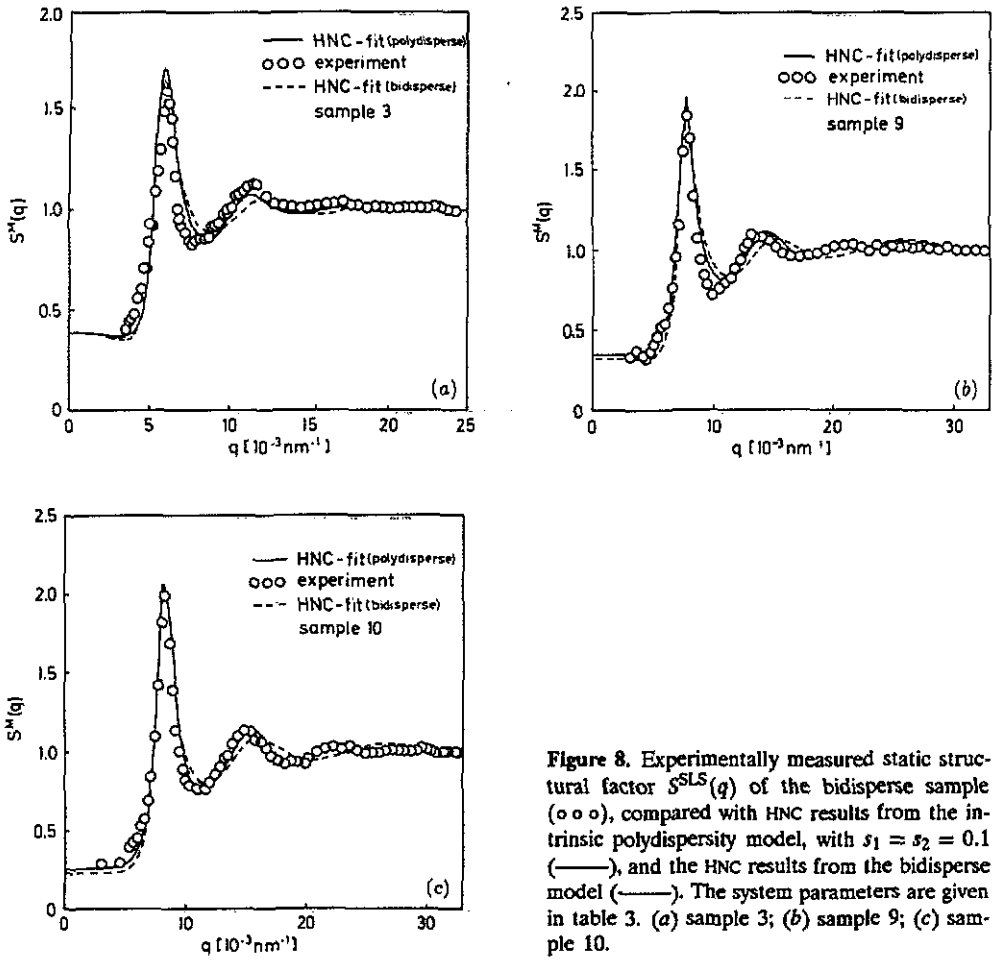

Figure 8. Experimentally measured static structural factor $S^{SLS}(q)$ of the bidisperse sample (o o o), compared with HNC results from the intrinsic polydispersity model, with $s_1 = s_2 = 0.1$ (———), and the HNC results from the bidisperse model (– – –). The system parameters are given in table 3. (*a*) sample 3; (*b*) sample 9; (*c*) sample 10.

The effective valencies Z_α^{theory}, $\alpha = 1,2$, used in our theoretical calculations of $S^M(q)$ were determined by adapting the peak height of the calculated structural factors $S^{theory}(q)$ of each pure sample to the experimentally observed ones. A good overall agreement is found between $S^{SLS}(q)$ and $S^{theory}(q)$ for all bidisperse samples, keeping fixed the effective valencies Z_α^{theory}, so determined.

It turns out that the extended RMSA, the hypernetted chain and Rogers–Young approximations are quite useful as fitting devices for strongly coupled binary systems. In particular the extended RMSA gives quick answers due to its analytical nature, whereas the HNC and RY approximations are more reliable for the particle and suspension characterization.

With the intrinsic polydispersity model, in which the particle size distribution was described by the Schulz distribution, we where able to reproduce the fine details of the measured structural factors in a satisfactory way. This last comparison shows that the measured $S^M(q)$ at small q values are dominated by the sample bidispersity and that, at the same time, the behaviour of $S^M(q)$ at large q values are mainly determined by the intrinsic polydispersity of each component.

Acknowledgments

We thank H Ruiz-Estrada and M Medina-Noyola for the supply of the extended RMSA program. This work has been supported by the Deutsche Forschungsgemeinschaft (SFB306). One of us (J M M-A) acknowledges a fellowship from the Deutsche Akademische Austauschdienst (DAAD).

References

[1] Pusey P N 1978 *J. Phys. A: Math. Gen.* **11** 119
[2] Grüner F and Lehmann W 1979 *J. Phys. A: Math. Gen.* **12** 303
[3] Grüner F and Lehmann W 1982 *J. Phys. A: Math. Gen.* **15** 2847
[4] Härtl W, Versmold H, Wittig U and Marche V 1983 *Molec. Phys.* **50** 815
[5] Hess W and Klein R 1983 *Adv. Phys.* **32** 173
[6] van Megen W and Snook I 1984 *Adv. Coll. Interface Sci.* **21** 119
[7] Ruiz-Estrada H and Medina-Noyola M and Nägele G 1990 *Physica* A **168** 919
[8] Krause R, Arauz-Lara J L, Nägele G, Ruiz-Estrada H, Medina-Noyola M, Weber R and Klein R 1991 *Physica* A in press
[9] D'Aguanno B and Klein R 1990 *J. Chem. Soc. Faraday Trans.* **86**
[10] Ackerson B J 1976 *J. Chem. Phys.* **64** 242
[11] Ackerson B J 1978 *J. Chem. Phys.* **69** 684
[12] Krause R, Nägele G, Karrer D, Schneider J, Klein R and Weber R 1988 *Physica* A **153** 400
[13] Hansen J P and McDonald I R 1986 *Theory of Simple Liquids* (London: Academic)
[14] van Megen W and Snook I 1977 *J. Chem. Phys.* **66** 813
[15] Frenkel D, Vos R J, de Kruif C G and Vrij A 1986 *J. Chem. Phys.* **84** 4625
[16] Hansen J P and Hayter J B 1982 *Mol. Phys.* **46** 651
[17] Nägele G, Medina-Noyola M, Arauz-Lara J L and Klein R 1987 *Prog. Coll. Polymer Sci.* **73**
[18] Genz U and Klein R 1991 *Physica* A in press
[19] Gaylor K and Snook I and van Megen W 1981 *J. Chem. Phys.* **75** 1682
[20] Kremer K and Grest G S and Robbins M O 1987 *J. Phys. A: Math. Gen.* **20** L181
[21] Kremer K (Johannes Gutenberg-Universität, Mainz, FRG) private communications
[22] Rogers F J and Young D A 1984 *Phys. Rev.* A **30** 999
[23] Méndez-Alcaraz J M, D'Aguanno B and Klein R 1991 *Physica* A submitted
[24] Moonen J A H M 1987 Small Angle Scattering of Colloidal Dispersions *PhD Thesis* Utrecht
[25] Wagner N J and Krause R and Rennie A R and D'Aguanno B and Goodwin J 1991 *J. Chem. Phys.* in press
[26] Vrij A 1982 *J. Colloid Interface Sci.* **90** 110
[27] Härtl W, Segschneider C, Versmold H and Linse P preprint